Supporting Information

Leppänen et al. 10.1073/pnas.0914318107

SI Text

Materials and Methods. ***Protein expression and purification.*** To produce human vascular endothelial growth factor VEGF-C in Sf9 insect cells, residues 112–215 (GenBank accession number X94216) followed by a hexahistidine tag were cloned into the pFASTBAC (Gibco) baculovirus transfer vector. Recombinant baculovirus was produced in Sf9 cells in serum-free Insect-Express (Lonza) medium supplemented with 50 μg/mL gentamicin (Sigma) at 27 °C. For protein expression, Sf9 cells were infected with recombinant VEGF-C baculovirus at high multiplicity and at 3 days after infection, the supernatant was harvested by centrifugation and VEGF-C was extracted by Ni^{2+} charged chelating sepharose (GE Healthcare) in batch. The resin was washed with PBS containing 15 mM imidazole and VEGF-C was eluted with 500 mM imidazole in PBS. Finally, VEGF-C was purified by gel filtration on a Superdex 200 (GE Healthcare) column in Hepes-buffered saline (HBS) (10 mM Hepes, 0.1 M NaCl) at pH 7.5. The VEGF-C Cys137Ala mutant and VEGF-A_{165} (1) were expressed and purified similarly. Soluble, dimeric VEGFR-2 [D2Fc, D23Fc, and D123Fc; domain 2, domains 2–3 (residues 118–326), and 1–3, respectively, fused to IgGFc] were prepared as described (2). N-terminal sequencing revealed that the N terminus for VEGFR-2 was the Asp120 residue, whereas the first distinct VEGF-C N-terminal residue was His113. A Factor Xa cleavage site allowed the Fc-tag removal.

The VEGF-C/VEGFR-2D23Fc complex was prepared by expressing the proteins separately in insect cells and mixing the culture supernatants in a 1:2 ratio. The clarified supernatant was loaded onto a Protein A sepharose CL-4B (GE Healthcare) column and, following an extensive wash with PBS, the complex was eluted with 0.1 M Glycine, pH 3.0. For Fc-tag removal, the buffer was immediately adjusted to PBS and the complex was incubated overnight at room temperature with 10 U Factor Xa (GE Healthcare) per 1 mg of the complex. Finally, the VEGF-C/VEGFR-2D23 complex was purified by gel filtration on a Superdex 200 (GE Healthcare) column in HBS (pH 7.5) and visualized on SDS-PAGE gels. The molecular weight of the VEGF-C/VEGFR-2D23 complex was measured by real-time multiangle laser light scattering during a Superdex 200 gel filtration. The measured 78.0 kDa molecular weight is consistent with the 2:2 stoichiometry because the calculated molecular weight without glycosylation is 72 kDa.

VEGFR-2D23 mutagenesis. Unique restriction sites AleI, BamHI, and BstEII in the pFASTBAC/VEGFR-2D23Fc baculovirus transfer vector were used to generate the VEGFR-1/-2 chimeric proteins by subcloning synthetic gene fragments (Geneart). Chimeric proteins C1–C5 bear VEGFR-1 amino acids EMYSEIPEIIH in residues 127–137 (human VEGFR-2 numbering), KKFPLDT in 162–169, LTHRQT in 215–220, TRVQ in 254–257, and IDQSNSHANI in 276–287, respectively. The Fc-tagged VEGFR-2 mutants were expressed in Sf9 insect cells and purified as above.

Cell survival assay. VEGFR-2/BaF3 cells express a chimeric receptor consisting of the extracellular domain of mouse VEGFR-2 fused to the transmembrane and intracellular domains of mouse erythropoietin receptor. The cells survive by the addition of VEGFR-2 ligands VEGF-C and VEGF-A, and their survival was quantified using an MTT [3-(4,5-dimethylthiazol-2-yl)-2,5-diphenyl tetrazolium bromide] substrate resulting with a color development (1). The survival of VEGFR-2/BaF3 cells was inhibited by simultaneous addition of either VEGF-C (100 ng/mL) or VEGF-A_{165} (30 ng/mL) and the soluble VEGFR-2 constructs. The cells were incubated at 37 °C for 48 h prior to the MTT assay. Background levels without either VEGF-C or VEGF-A stimulation were subtracted from the presented data points.

Binding studies. VEGF-C (Cys137Ala mutant) and VEGF-A_{165} isothermal calorimetric titrations to the soluble Fc-tagged VEGFR-2 constructs, and its mutants C3–C5, were carried out at 25 °C using VP-ITC calorimeter (MicroCal). To control for heat dilution effects, all the protein buffers were adjusted to HBS at pH 7.5. VEGFR-2 constructs were used in the calorimeter cell at a concentration of 5–10 μM, and the VEGF ligands in the syringe at 0.15–0.25 mM. Following the ITC titrations, the samples were visually analyzed for aggregation and the complex formation was confirmed by a size-exclusion chromatography step (Superdex 200 HR10/300, 10 mM Hepes, pH 7.5, 100 mM NaCl) followed by a SDS-PAGE analysis with silver staining. Data were processed using the MicroCal Origin 7.0 software.

VEGF-C (Cys137Ala mutant) and VEGF-A_{165} binding to the VEGFR-2, and its mutants C1–C5, were analyzed with surface plasmon resonance in the Biacore 2000 biosensor (GE). CM5 biosensor chip flow cells were covalently coated with the Fc-tagged VEGFR-2D23 variants via standard amine coupling. The binding was analyzed in running buffer of 10 mM Hepes, pH 7.4, 100 mM sodium chloride. The kinetics of the VEGF-C and -A interaction with VEGFR-2 and its mutants were determined by varying the ligand concentrations (20–2,560 nM) over a surface to which 2,000 resonance units of the receptors had been coupled. The contact time of VEGF molecules was 4 min and the flow rate 30 μL/min. The flow cells were regenerated after every injection with 10 mM Glycine, pH 1.7. The data were evaluated by first subtracting the sensorgram obtained from the empty control flow cell from the sensorgrams of the flow cells containing VEGFR-2 proteins. The response units at steady-state binding level of each individual concentration of VEGF molecules were plotted versus concentration and fitted (SigmaPlot 8.0 software package) assuming 1:1 binding to obtain dissociation constant K_d.

Crystallization and structure determination. For crystallization, the purified complex was concentrated to 3–5 mg/mL and the protein buffer (HBS) was supplemented with 0.01% (vol/vol) P8340 protease inhibitor cocktail (Sigma) and 0.01% (wt/vol) NaN_3. Crystallization conditions were screened using the sitting-drop vapor-diffusion technique. Two crystal types were identified in almost the same conditions. The orthorhombic VEGF-C/VEGFR2-D23 complex crystals grew within 1 to 3 weeks at 4 °C over a reservoir solution of 100 mM MES buffer, pH 5.0–5.6, 50 mM CsCl, and 28-32% (wt/vol) Jeffamine 600. The tetragonal crystals grew within 1 to 3 weeks at 4 °C over a reservoir solution of 100 mM Na-acetate buffer, pH 4.4–4.8, 50 mM CsCl, and 28–32% (wt/vol) Jeffamine 600. The final drops were prepared by manually mixing 1–2 μL of the reservoir solution and 1–2 μL of the protein solution. The orthorhombic crystals belong to space group $P2_12_12_1$ ($a = 73.8$, $b = 123.8$, and $c = 211.8$ Å) with two full complexes per asymmetric unit and solvent content of 50% (Table S1). The tetragonal crystals belong to space group $P4_22_12$ ($a, b = 88.7$ and $c = 105.7$ Å) with only half of the complex (one VEGF-C and one VEGFR2D23 chain) per asymmetric unit and solvent content of 57% (Table S1). For heavy-atom derivative data

collection, the orthorhombic crystals were soaked in 2 mM K_2PtCl_4 and the tetragonal crystals in 1% (vol/vol) saturated solution of CH_3HgAc at 0.1 M MES buffer, pH 5.5 for 2 hours. For data collection, the crystals were flash frozen in liquid nitrogen in the reservoir solution with 35% Jeffamine 600.

Complete datasets to 2.7 and 3.1 Å resolution were collected from single orthorhombic and tetragonal crystals, respectively, at the beam line X06SA at the Swiss Light Source (SLS) (Table S1). For phasing, anomalous data on the orthorhombic Pt-derivative were collected to 3.6 Å resolution at the beam line X06DA (SLS; Table S1). Data were processed with XDS (3) and the CCP4 suite of programs (4). SHELXC/D/E programs implemented in the HKL2MAP (5) graphical user interface were used to find 14 Pt sites and refine the anomalous and isomorphous differences, producing a phase set with a figure of merit of 0.51 at 2.8 Å. Experimental phases were further improved and extended by solvent flattening, histogram matching, and 4-fold noncrystallographic symmetry averaging with the program DM (4). The resulting electron density map allowed tracing the first VEGF-C and VEGFR-2D23 chains and the rest were located with Molrep (6) to complete the model. Two solvent molecules with anomalous signal were assigned as Cs ions. The phases were then input for iterative refinement in Refmac (4)/Phenix (7) with translation/libration/screw refinement and manual model building in Coot (8). Of the two independent complexes in the orthorhombic crystal form, complex 1 consists of VEGF-C chains A and B and the receptor chains M and N. The corresponding chains in complex 2 are C and D and L and O, respectively. The final VEGF-C models comprise residues A116-213, B117-214, C119-215, and D117-215. In each VEGF-C monomer, two glycan chains are present consisting of two *N*-acetyl-glucosamines and one mannose moiety (Asn175 and Asn205). The final VEGFR-2 models comprise residues M134-202, M210-264, M269-279, M283-326, N124-126, N132-265, N270-326, L123-128, L133-204, L208-326, O123-127, O132-2635, O269-280, and O282-325. The complex structure in the tetragonal crystal form, an Hg-derivative, was solved by molecular replacement using the structures from the orthorhombic crystal type as a search model. The structure was refined in Refmac (4) together with manual model building in Coot (8). The final VEGFR-2 model comprises residues R122-127, R130-205, and R208-326. The final VEGF-C model comprises residues E113-215. A 5% subset for the orthorhombic and a subset of 10% for the tetragonal crystal form of the diffraction data were omitted from refinement for calculating the free *R* factor (R_{free}). Stereochemical properties were assessed by MOLPROBITY (9). The final statistics of the structure solution and refinement are given in Table S1. Superpositions were calculated using the computer-graphics program MOLOC (10) and electrostatic surface potentials with the program DelPhi (11). Buried surface areas were calculated using Areaimol (4) by subtracting the total surface of the interacting molecules from the sum of the surfaces of the individual molecules. All figures were prepared using the program PyMol (http://pymol.sourceforge.net).

Comparison with the VEGF/VEGFR-2 EM structure. The two complexes in the asymmetric unit were converted into density volumes filtered to 25 Å resolution using the Bsoft software package (12) (Fig. S7*B* and *E*). The volumes where then used to calculate projections at an angular interval of 10° with the SPIDER image processing suite (13). The projections with the most similar features to the experimental 2-D averages by Ruch et al. (14) were selected (Fig. S7*C* and *F*).

1. Anisimov A, et al. (2009) Activated forms of VEGF-C and VEGF-D provide improved vascular function in skeletal muscle. *Circ Res* 104:1302–1312.
2. Jeltsch M, et al. (2006) Vascular endothelial growth factor (VEGF)/VEGF-C mosaic molecules reveal specificity determinants and feature novel receptor binding patterns. *J Biol Chem* 281:12187–12195.
3. Kabsch W (1993) Automatic processing of rotation diffraction data from crystals of initially unknown symmetry and cell constants. *J Appl Cryst* 26:795–800.
4. CCP4 (1994) The CCP4 suite: Programs for protein crystallography. *Acta Cryst D* 50:760–763.
5. Schneider TR, Sheldrick GM (2002) Substructure solution with SHELXD. *Acta Cryst D*58:1772–1779.
6. Vagin A, Teplyakov A (2000) An approach to multi-copy search in molecular replacement. *Acta Cryst D* 56:1622–1624.
7. Adams PD, et al. (2002) PHENIX: Building new software for automated crystallographic structure determination. *Acta Cryst D* 58:1948–1958.
8. Emsley P, Cowtan K (2004) Coot: Model-building tools for molecular graphics. *Acta Cryst D* 60:2126–2132.
9. Davis IW, et al. (2007) MolProbity: All-atom contacts and structure validation for proteins and nucleic acids. *Nucleic Acids Res* 35:375–383.
10. Gerber PR, Muller K (1995) MAB, a generally applicable molecular force field for structure modelling in medicinal chemistry. *J Comput Aided Mol Des* 9:251–268.
11. Rocchia W, et al. (2002) Rapid grid-based construction of the molecular surface and the use of induced surface charge to calculate reaction field energies: Applications to the molecular systems and geometric objects. *J Comput Chem* 23:128–137.
12. Heymann JB, Belnap DM (2007) Bsoft: Image processing and molecular modeling for electron microscopy. *J Struct Biol* 157:3–18.
13. Frank J, et al. (1996) SPIDER and WEB: Processing and visualization of images in 3D electron microscopy and related fields. *J Struct Biol* 116:190–199.
14. Ruch C, Skiniotis G, Steinmetz MO, Walz T, Ballmer-Hofer K (2007) Structure of a VEGF-VEGF receptor complex determined by electron microscopy. *Nat Struct Mol Biol* 14:249–250.

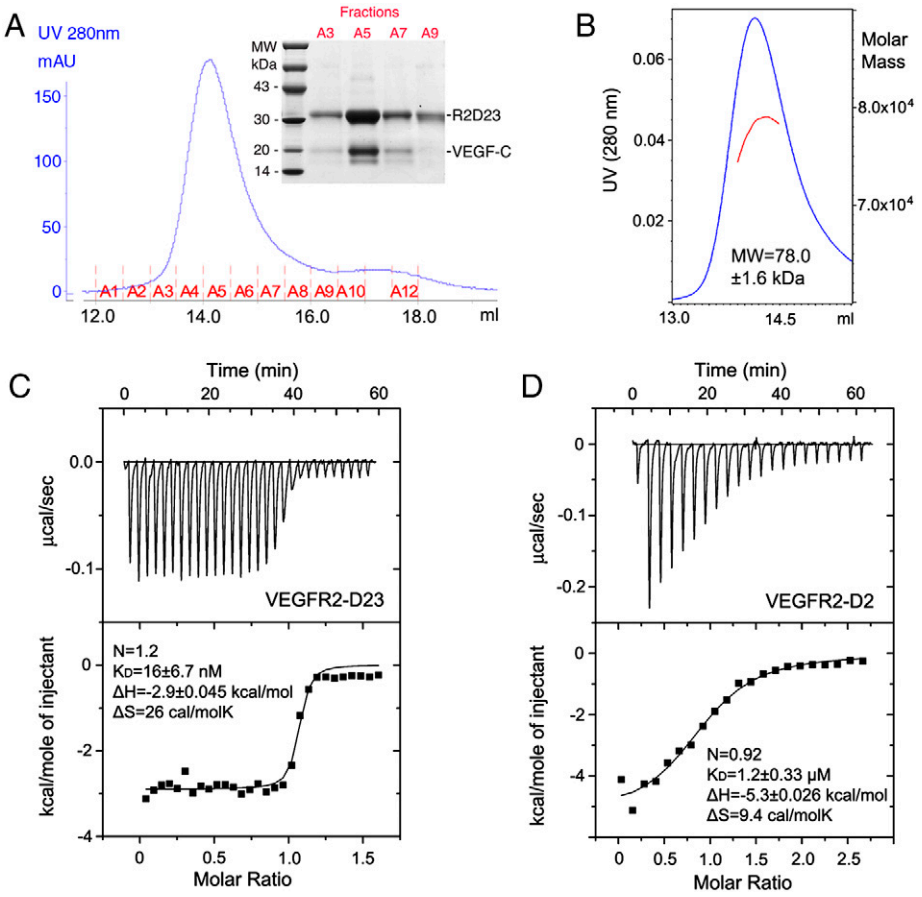

Fig. S1. Biochemical characterization of the VEGF-C/VEGFR-2 complex in solution. (*A*) A gel filtration analysis of the VEGF-C/VEGFR-2D23 complex on a Superdex-200 column. (*Inset*) SDS-PAGE showing that VEGF-C and VEGFR-2D23 (R2D23) coelute in the major peak. (*B*) Measurement of the molecular weight of the VEGF-C/VEGFR-2D23 complex by real-time MALS during a Superdex 200 gel filtration. (*C*) and (*D*) Isothermal titration calorimetry of VEGF-C with the Fc-tagged VEGFR-2D23 and VEGFR-2D2, respectively. The stoichiometry (*N*), affinity ($K_d \pm$ SD), enthalpy change ($\Delta H \pm$ SD), and entropy change (ΔS) of the binding experiments are shown.

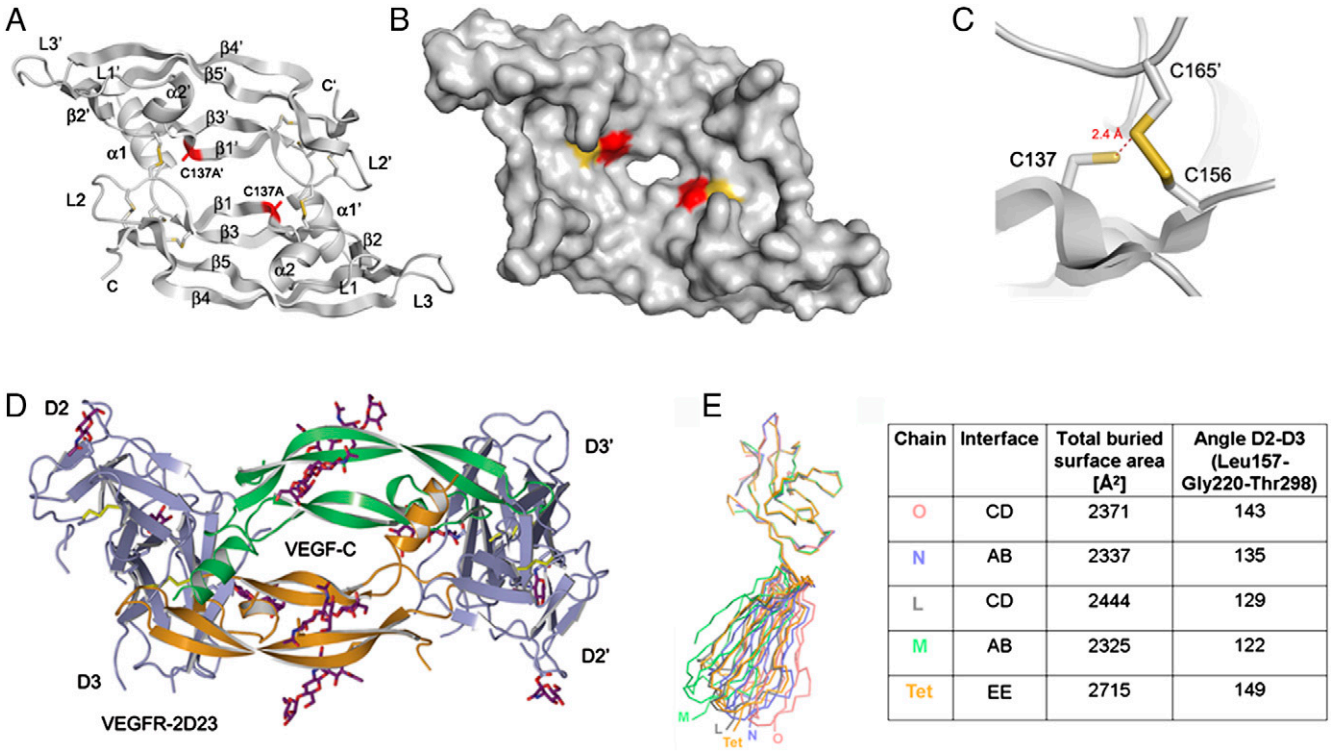

Chain	Interface	Total buried surface area [Å²]	Angle D2-D3 (Leu157-Gly220-Thr298)
O	CD	2371	143
N	AB	2337	135
L	CD	2444	129
M	AB	2325	122
Tet	EE	2715	149

Fig. S2. VEGF-C Cys137Ala mutant structure and variation in VEGFR-2 D23 chains. (*A*) A main-chain representation of the VEGF-C Cys137Ala mutant in the VEGFR-2D23 complex. The Cys137Ala (C137A) mutation site is labeled and highlighted in red. Secondary structure elements and loops L1–L3 are labeled. VEGF-C loop L1, between the strands β1 and β3, includes a short β-strand (β2) and an α-helix (α2). The disulfides in the cystine-knotmotif are shown in yellow. (*B*) The same as in (*A*) with surface representation. (*C*) Close up of (*A*) with residue 137 modeled as cysteine according to the WT VEGF-C sequence. The Cys137 free thiol is close to the Cys156–Cys165′ interchain disulfide bridge. (*D*) Structure of the VEGF-C/VEGFR-2D23 complex in a cartoon representation. The VEGF-C homodimer is shown in orange and green, and the two VEGFR-2 receptor chains are colored in light blue. The sugar moieties and the disulfide bonds are shown in purple and yellow sticks, respectively. A top-down view toward the cell surface. The VEGFR-2 domains around the VEGF-C have an orientation of a left-handed twist. (*E*) Comparison of the VEGFR2-D23 chains in the orthorhombic (L-O) and in the tetragonal (Tet) crystal forms of the VEGF-C complex structure and implications on the binding interface. The five VEGFR-2D23 chains (L-O, Tet) show differences in D3 orientation relative to D2 and to the bound VEGF-C. Total buried surface areas are listed for the five independent VEGF-C/VEGFR-2D23 interfaces. Also, the different bending angles between the VEGFR-2 domains 2 and 3 are given.

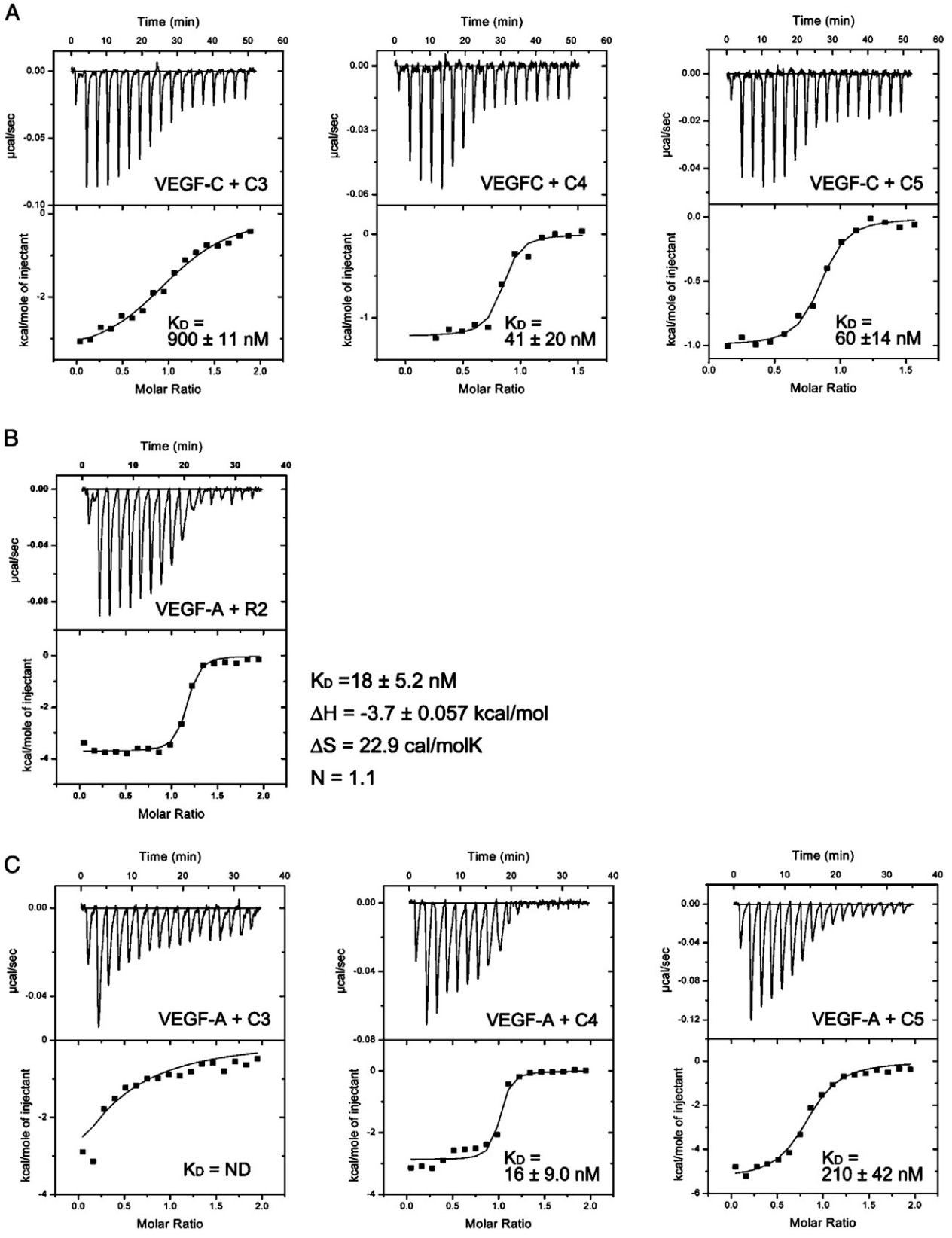

Fig. S3. Thermodynamic analysis of VEGF-C and -A interactions with the VEGFR-2D23 variants. (*A*) Calorimetric titration of VEGF-C (C137A mutant) to the three VEGFR-1/-2 chimeric proteins (C3–C5). (*B*) VEGF-A_{165} titration to the Fc-tagged VEGFR-2D23 together with the stoichiometry (*N*), affinity ($K_D \pm$ SD), enthalpy change ($\Delta H \pm$ SD), and entropy change (ΔS) of the binding experiment. (*C*) VEGF-A_{165} titration to the VEGFR-1/-2 chimeric proteins. ND, not determinable.

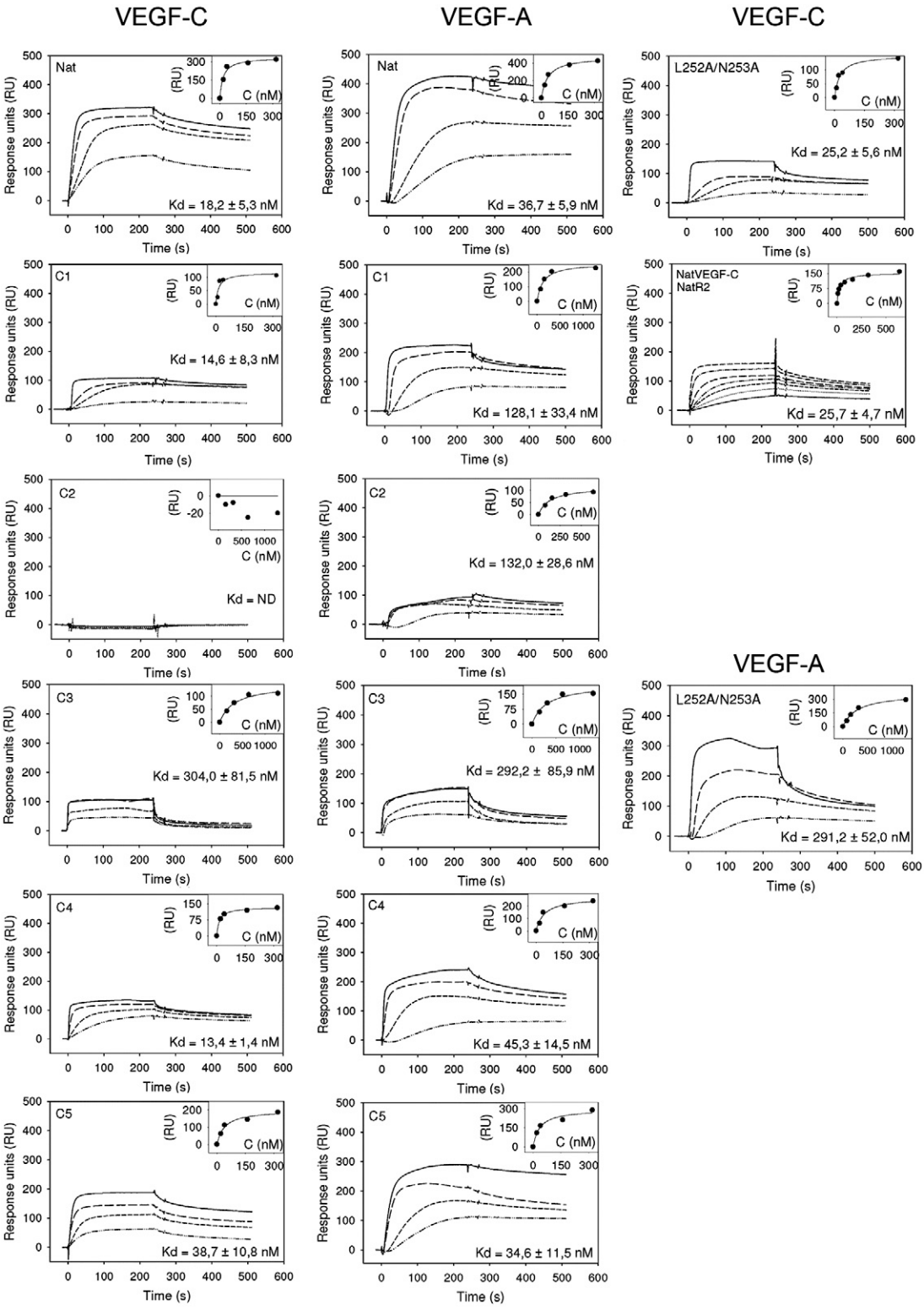

Fig. S4. Surface plasmon resonance analysis of VEGF-C and VEGF-A interactions with the VEGFR-2D23 variants. Surface plasmon resonance (Biacore) sensorgrams of VEGF-C (C137A mutant) and VEGF-A_{165} binding to the Fc-tagged native VEGFR-2D23 (Nat), VEGFR-1/-2 chimeric proteins (C1–C5), and to the VEGFR-2D23 double mutant L252A/N253A. Native VEGF-C (NatVEGF-C) interaction with the Fc-tagged native VEGFR-2D23 (NatR2) was also studied. Sensorgrams obtained from empty control flow cells were subtracted from the shown sensorgrams. Data are expressed as $K_D \pm$ SD. ND, not determinable.

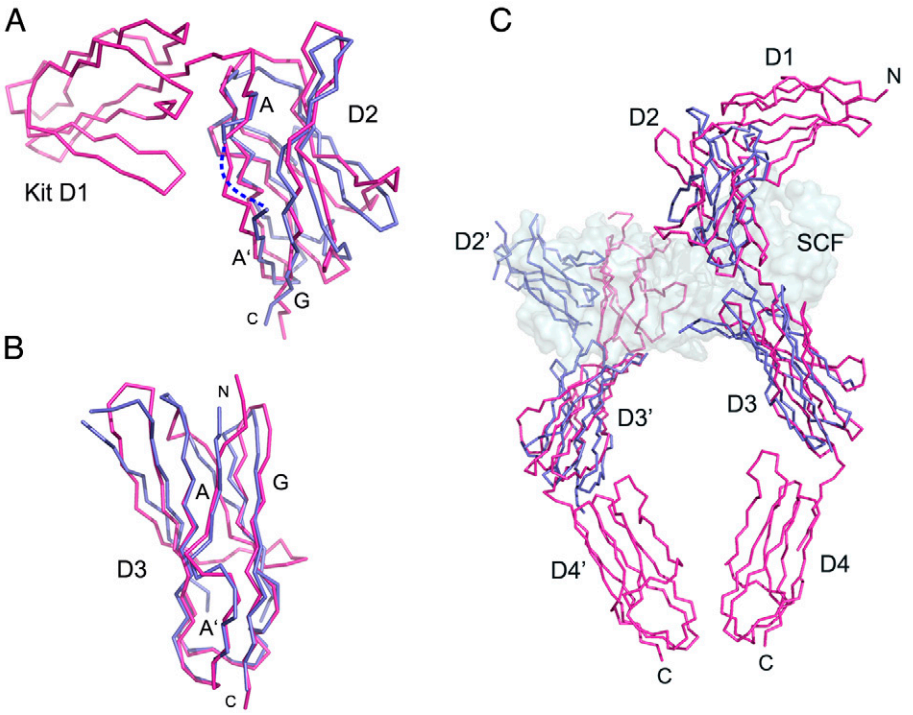

Fig. S5. Structural comparison of the VEGF-C/VEGFR-2D23 and the SCF/Kit complexes (PDB code 2E9W). VEGFR-2 (*Blue*) and Kit (*Magenta*) receptors are shown in ribbon diagram. (*A*) Superposition of the VEGFR-2 and Kit structures on base of the D2 domains (rmsd of 2.3 Å for 74 Cα atoms). Strands A, A′, and G are labeled. VEGFR-2 disordered residues 128–132 between the D2 strands A and A′ are depicted with a dashed line. (*B*) Superposition of VEGFR-2D3 and Kit D3 structures (rmsd of 1.6 Å for 89 Cα atoms). Strands A, A′, and G are labeled. (*C*) Superposition of the complexes on base of the receptor D23 domains. SCF in the Kit complex is shown as a semitransparent surface colored in cyan. For clarity, only Kit domains D1–4 and D2′–4′ are shown. VEGFR-2D23 and Kit D23 domains show variation D23 bending angle.

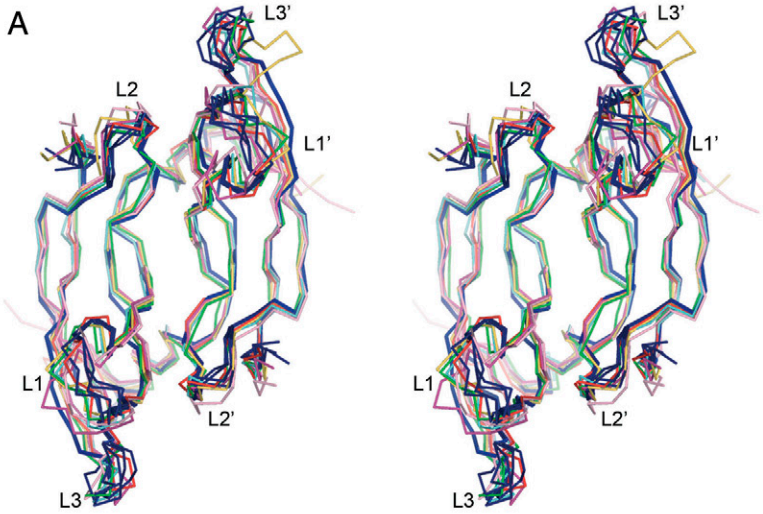

B

VEGF	Number of residues	r.m.s.d. [Å]	Sequence identity [%]
VEGF-C (chain AB on CD)	192	1.01	100
VEGF-C (chain AB on DC)	192	0.73	100
VEGF-C (chain DC on CD)	192	1.08	100
VEGF-A (PDB-code 1FLT)	144	1.35	33
VEGF-B (PDB-code 2C7W)	134	1.85	28
VEGF-B (PDB-code 2VWE)	136	1.79	28
VEGF-E (PDB-code 2GNN)	136	1.68	31
PlGF (PDB-code 1RV6)	150	1.53	29
VR-1 (PDB-code 1WQ9)	152	2.03	22

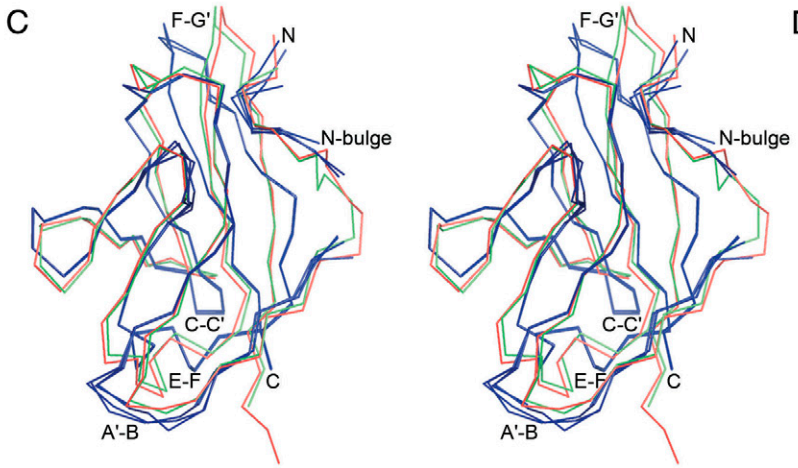

D

Receptor	Number of residues	r.m.s.d. [Å]
VEGFR2-D2 (chain L on O)	79	0.31
VEGFR2-D2 (chain M on O)	77	0.74
VEGFR2-D2 (chain N on O)	85	0.33
VEGFR1-D2 (chain X on O)	68	2.20
VEGFR1-D2 (chain X on N)	67	2.12
VEGFR1-D2 (chain X on M)	53	2.02
VEGFR1-D2 (chain X on L)	57	1.90

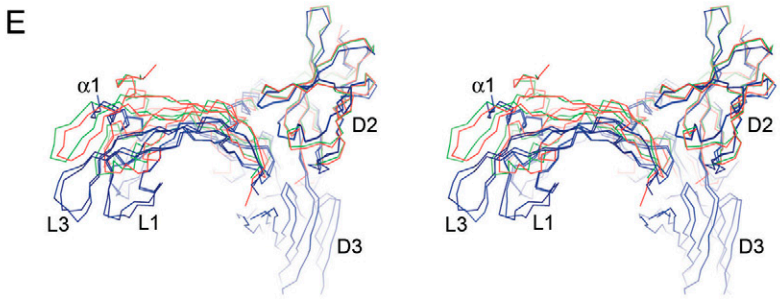

Fig. S6. Structural comparison of the VEGF family ligands and their receptor complexes. (*A*) Superposition of the VEGF family ligand structures. VEGF-C chains are in blue. (*B*) Superposition statistics for the VEGF family ligands using the same color code for the different VEGFs as in (*A*). VEGF-C shares 22–33% sequence identity with the other VEGF family members of known structure and can be superimposed onto these dimeric structures with rmsd between 1.4 and 2.0 Å. (*C*) Superposition of the D2 domains of the VEGF-C/VEGFR-2D23 (*Blue*), VEGF-A/VEGFR-1D2 (*Orange*; PDB code 1FLT), and PLGF/VEGFR-1D2 (*Green*; PDB code 1RV6) complexes. (*D*) Superposition statistics for the VEGF receptor D2 domains. The ligand binding domains of human VEGFR-1 and VEGFR-2 share 31% sequence identity, and the D2 domains can be superimposed onto VEGFR-1D2 with rmsd of 1.9-2.2 Å. (*E*) Superposition of the D2 domains as in (*C*) showing the different relative orientations of the ligands toward the D2 domains. The same color code is used.

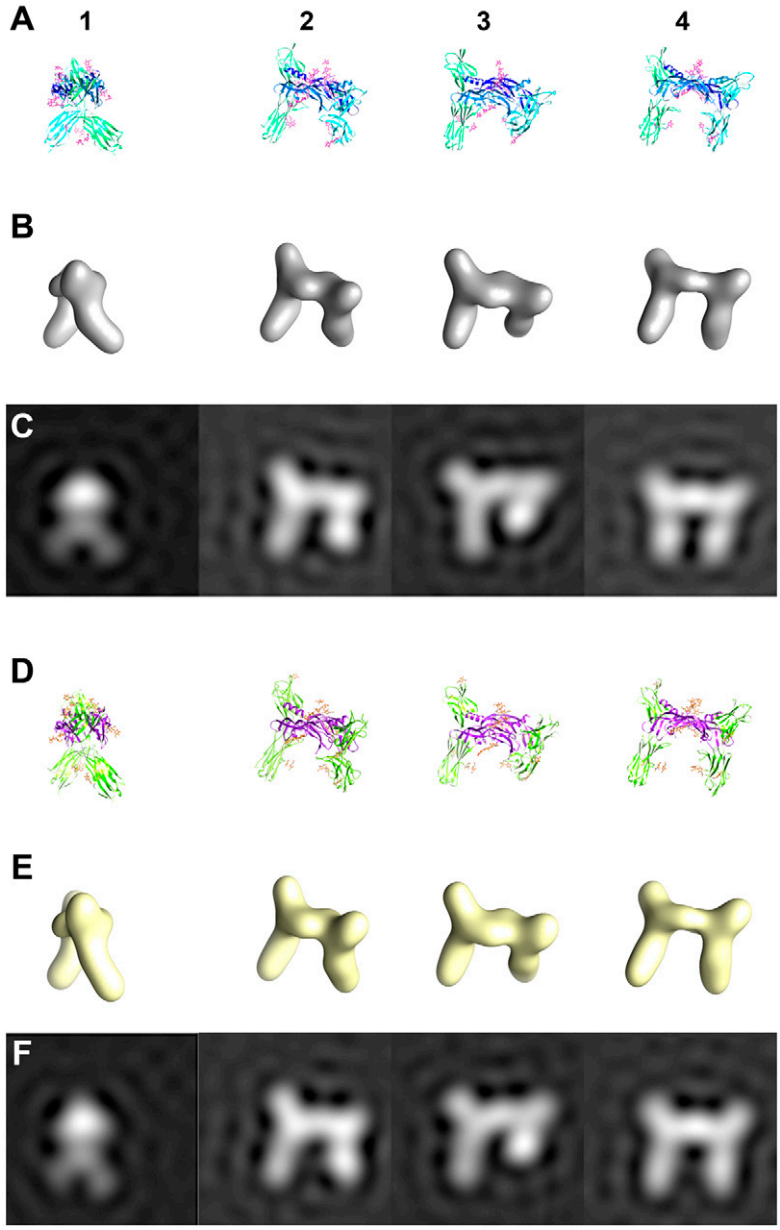

Fig. S7. Comparison of the two VEGF-C/VEGFR-D23 complexes and the VEGF-A/VEGFR-2 EM model. (*A*) Ribbon representation of complex 1 in four different orientations, which were chosen according to the calculated projections that show the most similar features to the experimental 2D EM averages by Ruch et al. (14). (*B*) Calculated volumes of complex 1 filtered at 25 Å resolution. (*C*) Corresponding projections. (*D*), (*E*), and (*F*) Same as in (*A*), (*B*), and (*C*), but for complex 2. The orientations correspond to the following 2-D EM averages (14): 1, panel 2 in Fig. 1*C* and panel 6 in Fig. 2*A*; 2, panel 3 in Fig. 1*C*; 3, panel 3 in Fig. 2*A*; 4, panel 5 in Fig. 2*A*.

Table S1. Data collection and refinement statistics

	Native 1*	Pt-derivative*	Native 2*
Data collection			
Space group	$P2_12_12_1$	$P2_12_12_1$	$P4_22_12$
Cell dimensions			
a, b, c, Å	73.8, 123.8, 211.8	73.7, 123.6, 211.6	88.7, 88.7, 105.7
α, β, γ, °	90.0, 90.0, 90.0	90.0, 90.0, 90.0	90.0, 90.0, 90.0
Resolution, Å	80-2.7 (2.8–2.7)†	60-3.6 (3.8–3.6)†	37-3.1 (3.2–3.1)†
R_{merge}	6.9 (73.4)	8.7 (24.7)	9.5 (55.2)
I/σ*	20.1 (2.8)	15.9 (5.8)	29.2 (7.5)
Completeness, %	99.6 (99.5)	99.5 (97.6)	99.9 (100.0)
Redundancy	6.7	3.9	17.3
Refinement			
Resolution, Å	53-2.7		37-3.1
No. reflections	53,953		8,092
R_{work}/R_{free}	22.5/27.7		25.7/34.6
No. atoms			
Protein	9002		2476
Carbohydrate	547		137
Cs ion	2		
Hg ion			1
Water	191		30
B factors			
Protein	71.2		56.3
Carbohydrate	96.0		86.1
Cs ion	104.7		
Hg ion			142.6
Water	52.8		30.2
rmsd from ideal values			
Bond lengths, Å	0.005		0.006
Angles, °	1.000		1.068
Ramachandran plot			
Favored regions	94.6%		94.9%
Outliers	0.36%		1.0%

*A single crystal was used for each data set.

†Values in parentheses correspond to the highest resolution shell.

Table S2. Interactions between VEGF-C and VEGFR2-D23 for the four (A–D) VEGF-C chains in the orthorhombic crystal form and the one in the tetragonal form (E).

VEGF-C		VEGFR2-D23		
$VEGF\text{-}C_{chain}$		Hydrogen bonds and salt bridges (bold)	Van der Waals contacts	Domain
Conserved (A-E)	D123	**D123**($\mathbf{O^{\delta 1}}$)–**R164**($\mathbf{N^{\eta 1}}$) D123($O^{\delta 2}$)–Y165($O^{\eta 2}$)	M197	D2
	W126		Y165, G196, M197	D2
	R127		Y165	D2
	N167	N167($N^{\delta 2}$)–Y194(O)		D2
	E169	E169(N)–N253($O^{\delta 1}$) E169($O^{\epsilon 1}$)–N253(N) **E169**($\mathbf{O^{\epsilon 2}}$)–**K286**($\mathbf{N^{\zeta 1}}$)		D3
	G170		L252	D3
$N115_E$			Q132	D2
$L119_{A,B,E}$			M213	D2
$Q130_C$			Y165	D2
$Q130_{D,E}$		Q130($O^{\delta 1}$)–P166(N)	Y165	
$T148_A$		T148($O^{\gamma 1}$)–I256(O) T148(O)–I256(N)	N274, R275, F288	D3
$T148_B$		T148(N)–D276($O^{\delta 2}$) T148(O^{γ})–K286$N^{\zeta 1}$	F288	
$T148_C$		T148(O^{γ})–D276($O^{\delta 2}$)	D276	
$T148_D$		T148(O)–I256(N) T148(O^{γ})–I256(O)	N274	
$T148_E$			R275, F288	D3
$N149_A$		N149(N)–I257(O)	D257	D3
$N149_B$		N149($O^{\delta 1}$)–I256(N) N149($N^{\delta 2}$)–I256(O)		
$N149_{D,E}$		N149($N^{\delta 2}$)–D257($O^{\delta 1}$)	D257	
$F151_{A,B,D,E}$			G255 and/or N253, V254	D3
$K153_{A,D}$			I215	D2
$S168_{D,E}$			V218	D2
$F186_{B,C}$			I215	D2
$F186_{D,E}$			I215, H133	
I188			Y137 and/or V217	D2
$V190_{A,B,C,E}$			V217 or G255	D2 or D3
$P191_{A,B,C}$			G312 or G255	D3
$L192_{B,E}$			Y137	D2 or D3
$L192_C$			V219, Y137	
$L192_D$			G312	
$G195_D$		G195(O)-Y135(O^{H})		D2
$P196_{B,D,E}$			V135	D2

Hydrogen bonds and salt bridges were calculated using cutoff distances of 3.4 and 4.0 Å, respectively. The cutoff distance for van der Waals contacts was 4.0 Å.